Impact of contour on surface quality, dimensional and geometrical accuracy of Ti48Al2Cr2Nb parts produced with powder bed fusion with electron beam process

# Impact of contour on surface quality, dimensional and geometrical accuracy of Ti48Al2Cr2Nb parts produced with powder bed fusion with electron beam process

Giovanni RIZZA[1,a] *, Manuela GALATI[1,b], Paolo MINETOLA[1,c], Paolo ANTONIONI[1,d], Danilo BRUSON[1,e], Giovanni MARCHIANDI[1,f], Luca IULIANO[1,g]

[1]Department of Management and Production Engineering (DIGEP), Integrated Additive Manufacturing Center (IAM@PoliTo), Politecnico di Torino, Corso Duca degli Abruzzi 24, 10129 Torino, Italy

[a]giovanni.rizza@polito.it, [b]manuela.galati@polito.it, [c]paolo.minetola@polito.it, [d]paolo.antonioni@polito.it, [e]danilo.bruson@polito.it, [f]giovanni.marchiandi@polito.it, [g]luca.iuliano@polito.it

**Keywords:** Additive Manufacturing, Metrology and Tolerancing, Surfaces

**Abstract.** Powder bed fusion with electron beam (PBF-EB) is an additive manufacturing technique for processing critical materials such as Ti48Al2Cr2Nb. Most of these applications are focused on industrial components that require mirror-like finishing. Therefore, PBF-EB parts are considered only near net shape. The PBF-EB standard procedure involves melting using contours before the inner area. However, because of the need for machining allowance, using contours appears unnecessary, while it may increase the production time significantly. This work highlights the differences between Ti48Al2Cr2Nb parts produced using the standard procedure of PBF-EB and a counterpart produced with a modified single-stage melting. Surface topography, dimensional and geometrical accuracies and mechanical properties are compared. The results show that the parts produced with a single-stage melting are more accurate in dimensions than those produced using a standard strategy, while the production time is over 8% shorter.

## Introduction

The building conditions of the powder bed fusion with electron beam (PBF-EB) additive manufacturing process enable the production of materials that are difficult to process using traditional or other additive manufacturing techniques. One such example is the intermetallic γ titanium aluminide alloy [1]. This advantage is guaranteed by the high build process temperature and the vacuum environment in the build chamber [2]. The vacuum level is approximately $10^{-5}$ mbar, which is sufficient to prevent the backscatter of the electrons by the air molecules and allow the material to be processed without the risk of oxygen or nitrogen pickup [3]. With these processing conditions, γ-TiAl offers remarkable specific properties of strength, Young's modulus and creep resistance, particularly when compared to nickel alloys [2].

During the production of γ-TiAl, particularly the Ti48Al2Cr2Nb (Ti4822), the typical working temperature is between 1050°C and 1100°C [2]. At each layer, this temperature is reached thanks to the preheating step in which the electron beam scans the whole layer repeatedly till the desired temperature is reached. In addition, the vacuum environment , typical of the PBF-EB processes, inhibits the heat dispersion. During the preheating, the powder is partially sintered [4], improving the heat transfer between the melt pool and the surrounding material and in turn reducing the cooling rate of the melt pool [2]. The melting step for Ti4822 processed by PBF-EB consists of melting the section using parallel lines in one single step, identified as hatching. To the best of the authors' knowledge, Ti4822 has never been processed with the PBF-EB using the two-steps standard melting strategy, well established for other materials such as Ti6Al4V [5], [6], or

Materials Research Proceedings 57 (2025) 11-19 https://doi.org/10.21741/9781644903735-2

Ti6Al2Sn4Zr2Mo [7]. In this strategy, melting consists of two melting steps: the contour first and the inner or hatch after [3], [8]. The contour employs a distinctive melting strategy known as the Multibeam$^{TM}$ strategy. During Multibeam$^{TM}$, the PBF-EB machine control rapidly moves the electron beam in different contour locations, simultaneously activating several melt pools [9].

The literature suggests that the use of a contour prior to the hatching of the inner area affects only the surface roughness of the components, which is smaller for components produced using contours [10]. The reason for this difference is connected to the larger amount of energy usually delivered when melting the hatch than that delivered when melting the contour. However, given the requirements typically associated with γ-TiAl components in automotive or aerospace industries, additional machining operations are requested. Despite has already been showed in the literature the part quality issues associated with the PBF-EB production for titanium alloys, such as [11], all of these works are only based on the use of the two-step strategy, and no systematic comparison has been made with the one-step strategy. This paper covers this literature gap, investigating the differences between two-step and one-step strategies. Two artefacts were produced using the standard two-step and the one-step strategy. A comparison of the melting strategies was made considering the topography of the surfaces and the dimensional and geometrical tolerances.

## Materials and methods

To investigate the effect of the melting strategy, this work adopts two portions of the benchmark proposed by Minetola et al. [12] and the relative procedure for the measurements developed according to the standard ISO 286:1988 [13] and ISO 286-1:2010 [14]. The benchmark reference part is available as open access here [15]. Fig. 1 shows artefact 1 and artefact 2 adopted in this work.

The overall size of artefact 1 is 110 mm x 25 mm x 33 mm, while artefact 2 has an overall size of 55 mm x 55 mm x 21 mm. Artefacts 1 and 2 include features with sizes that are comprised in the basic size ranges of the ISO 286:1988 [13] and ISO 286-1:2010 [14]: from 1mm to 3 mm, from 3 mm to 6 mm, from 6 mm to 10 mm, from 10 mm to 18 mm, from 18 mm to 30 mm, from 30 mm to 50 mm, from 50 mm to 80 mm and from 80 mm to 120 mm. All these features are built on a supporting plate 5 mm thick. Each set of features is named with an alphabetic index, as shown in Fig. 1 and described below. On one side of artefact 1, there are seven rectangular steps (ST) with dimensions 4 mm x 15 mm. The height of these steps is 1 mm, 3 mm, 6 mm, 10 mm, 15 mm, 21 mm and 28 mm. The central portion of this artefact includes a rectangular block with dimensions 20 mm x 46 mm x 24 mm. This block contains seven rectangular slots (SL) with dimensions 5 mm x 15 mm. The depth of these slots is the same as the steps, except for the slot that is 3 mm deep, which is repeated twice. One side of this central block includes five planes tilted at different angles with respect to the vertical (TP). The first is vertical, the second is tilted at 2 degrees, the third at 4.5 degrees, the fourth at 7 degrees and the fifth at 9 degrees. Artefact 1 also contains seven rectangular blocks (BL) with dimensions of 4 mm x 15 mm separated by a 1 mm gap. The height of these blocks is the same as the steps. Artefact 2 contains two truncated cones with a circular base (TC1), one inside the other. The larger base of the external cone has a diameter of 20 mm, while the smaller base has a diameter of 13.6 mm. The height of this cone is 12 mm. The larger base of the inner cone has a diameter of 10 mm, while the smaller one has a diameter of 6.5 mm. The height of this cone is 10 mm. Artefact 2 also contains a series of coaxial cylinders (CC1). The larger cylinder has a diameter of 24 mm, while the smaller cylinder on top has a diameter of 17 mm. This feature contains two other cylinders with a diameter of 7 mm, the one on top and 5 mm, the one at the bottom. Each cylinder has a height of 8 mm. The last features are two series of quarters of convex and concave spheres (SP1 and SP2). The spheres of SP1 have a diameter of 24 mm, while the spheres of SP2 have a diameter of 16 mm. Artefacts 1 and 2 together allow the evaluation of more than one thousand dimensions in the ISO ranges of 1mm and 120 mm. The disposition of the feature also allows the evaluation with a coordinate measuring machine (CMM) using only one positioning of the sample and a probe of 2 mm in diameter.

The PBF-EB machine, Arcam A2X was adopted to produce artefacts 1 and 2. As mentioned above, the material adopted was the intermetallic Ti48Al2Cr2Nb alloy (Ti4822). The granulometry ranged between 45 µm and 150 µm. According to the literature [16], the layer thickness was selected as equal to 90 µm. Two replicas of artefacts 1 and 2 were produced: one replica for each melt strategy. Table 1 reports the process parameters adopted to melt outer and inner contours with Multibeam$^{TM}$ and hatch for the parts produced with the two-step strategy. The artefacts produced with the one-step strategy were produced using the parameters for the hatch reported in Table 1. No scaling factor was applied to nominal geometries of the samples. The four samples were produced in one build to ensure the same temperature conditions. At the end of the production, the samples were cleaned according to the standard procedure [3], [17] in a powder recovery system in which the breakaway powder was sandblasted using the same powder used in the PBF-EB process. No heat treatments or other post-process operations were performed on the artefacts produced. After extracting the samples from the build chamber of the machine, these were characterised topographically and dimensionally.

To evaluate the differences in the production time between the two melting strategies, two ad-hoc builds were designed in which only one melting strategy at a time was considered. The time for the production was estimated by using the EBM control of the machine. The simulator solely calculates the time required for preheating, the melting of the cross-section and the eventual post-heating/cooling at each layer. the simulator neglects the time for the powder ranking. This is a fixed time which do not depend on the melted material.

*Table 2. Process parameters adopted to melt the contour with Multibeam$^{TM}$ and hatch.*

| | Scan speed [mm/s] | Focus offset [mA] | Beam current [mA] | Number of spots | Number of contours | Contours offset[mm] |
|---|---|---|---|---|---|---|
| Outer contour | 440 | 6 | 5 | 40 | 1 | 0.25 |
| Inner contour | 800 | 6 | 10.2 | 15 | 2 | 0.25 |
| | Speed function | Focus offset [mA] | Beam current max [mA] | Reference length [mm] | Reference current [mA] | Line offset [mm] |
| Hatch | 40 | 15 | 20 | 18 | 7 | 0.3 |

The topography was investigated by inspecting peaks and valleys to highlight the differences in the melting strategy adopted. The topography of the samples was obtained through a structured light scanner ATOS compact scan (Carl Zeiss GOM Metrology GmbH, Braunschweig, Germany). The maximum resolution of the scanner is 0.018 mm. The cloud of points was handled using the software GOM inspect 2021 (Carl Zeiss GOM Metrology GmbH, Braunschweig, Germany), with no post-process. The software MountainsLab (Digital Surf, Besançon, France) was adopted to inspect topography characteristics, the average surface roughness (Sa) and the maximum height of surface (Sz). Horizontal surfaces are defined as all the surfaces parallel to the start plate. Vertical surfaces are orthogonal to the start plate and aligned with the build direction.

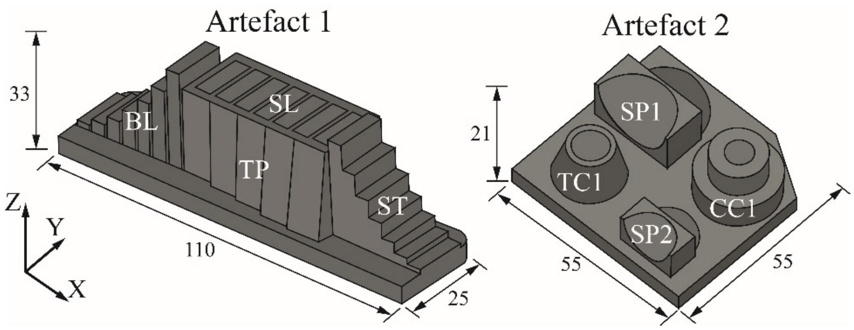


*Fig. 1. Artefact 1 and 2 adopted for the topographic, dimensional and geometrical characterisation. Z is aligned to the build direction.*

The dimensional accuracy was investigated by a CMM Altera S (LK Metrology Ltd., Derby, England). This machine has an accuracy envelope with an MPEE of 1.8 +L/400. Each artefact was measured three times, and the average measure was adopted for the analysis. The measures taken through the CMM were adopted to evaluate the standard tolerance factor according to the ISO guidelines [13]. The standard tolerance classes, from IT5 to IT18, for measures up to 500 mm, are a function of the standard tolerance factor i described by Eq. 1

$$i=0.45\sqrt[3]{D}+0.001D \quad (1)$$

Where $D=\sqrt{D_1 D_2}$ and $D_1$ and $D_2$ are the lower and the upper limits of the basic size range. Table 3 reports the value of the standard tolerance factor i calculated for each size range given by the ISO standard.

*Table 3. Standard tolerance factors for each basic size.*

| Range | Basic size | | | | | | | | |
|---|---|---|---|---|---|---|---|---|---|
| Above | $D_1$ (mm) | 1 | 3 | 6 | 10 | 18 | 30 | 50 | 80 |
| Up to and including | $D_2$ (mm) | 3 | 6 | 10 | 18 | 30 | 50 | 80 | 120 |
| Standard tolerance factor | i (μm) | 0.542 | 0.733 | 0.898 | 1.083 | 1.307 | 1.561 | 1.856 | 2.173 |

Table 4 reports the formulas adopted to assign a standard tolerance grade (IT) to a measure. This is assigned to a measure according to the number of times (n) the tolerance factor (i) fits the dimensional deviation of the measure from the nominal measure. The parameter n is evaluated according to Eq. 2.

$$n=1000\ \frac{|D_n-D_m|}{i} \quad (2)$$

Where $D_n$ and $D_m$ represent the nominal and the measured dimension, respectively.

*Table 4. Formulas to assign the standard tolerance (IT) grade to a measure, according to his deviation from the nominal.*

| Basic size | | Standard tolerance grades | | | | | | | | | | | | | |
|---|---|---|---|---|---|---|---|---|---|---|---|---|---|---|---|
| | | IT 5 | IT 6 | IT 7 | IT 8 | IT 9 | IT 10 | IT 11 | IT 12 | IT 13 | IT 14 | IT 15 | IT 16 | IT 17 | IT 18 |
| Above | Up to | Standard tolerance [μm] | | | | | | | | | | | | | |
| 1 mm | 500 mm | 7i | 10i | 16i | 25i | 40i | 64i | 100i | 160i | 250i | 400i | 640i | 1000i | 1600i | 2500i |

Materials Research Proceedings 57 (2025) 11-19 https://doi.org/10.21741/9781644903735-2

As an example, to clarify the use of Equation 1 and 2 and tables 3 and 4, assuming a nominal dimension $D_n$ = 40 mm and a measured dimension $D_m$ = 40.250, the standard tolerance factor for this dimension is i = 1.561 (from Table 3 and Equation 1) and the parameter n = 160.15 (Equation 2). With this value of n, the dimension can be classified as an IT13. In order to be classified as IT 12, a measure should have a deviation between 100 i (with n = 100) and 160 i (with n = 160).

Considering all the features of the artefacts, n will have a distribution in each basic ISO range size. In this work, the 95$^{th}$ percentile is assumed as the maximum error when producing a feature in the specific range size of Table 3. The measures taken with CMM were adopted to evaluate the geometric dimensioning and tolerancing (GD&T). In particular, the following factors were investigated: perpendicularity, cylindricity, angle of the planes, flatness of the planes for horizontal (parallel to the start plate), vertical (parallel to the build direction) and tilted with respect to the vertical planes, and parallelism between horizontal and vertical planes.

**Results and discussion**

Fig. 2 shows artefact 2 after the cleaning operation in the PRS. It also allows a visual comparison among the artefacts produced with the one-step (Figure 2 a)) and the two-step (Figure 2 b))strategy. The time calculated to produce samples with a two-step strategy was 2 hours and 50 minutes, while the time calculated to produce the artefacts with the one-step strategy was 2 hours and 37 minutes. The difference between the two melt strategies was 13 minutes. Therefore, the one-step strategy is approximately 8 % faster than the two-step strategy.

As can be observed in Fig. 2, the surface produced with the one-step strategy shows the presence of the layers, with the stair-stepping effect clearly visible. In the case of the two-step strategy, the stair-stepping and the layers are visible for the highest section of the sphere, where the molten cross-section becomes small.

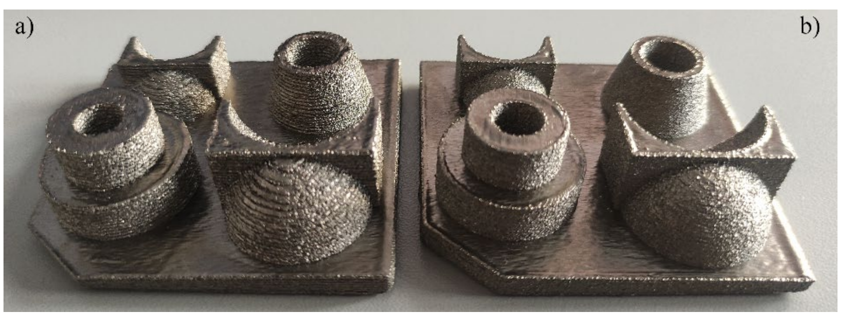


*Fig. 2. Artefact 2 produced using the a) one-step and b) the two-step strategy.*

Fig. 3 shows the results of the topography analysis on vertical surfaces of artefact 1 produced with the two-step strategy (Fig. 3 a)), and the one-step strategy (Fig. 3b)). As can be observed, the topography is substantially different. The first evidence is that the roughness of the surface is significantly affected by the contour. The surface melted with a two-step strategy is more regular with a less evident staircase effect due to the slicing operation. This evidence is confirmed quantitatively by the areal surface roughness measurements. The surface produced with the two-step strategy is characterised by a Sa = 31.44 µm and an Sz = 331.4 µm. On the other hand, the surface produced with the one-step strategy is characterised by Sa = 54 µm and Sz = 499 µm. The higher values of Sa and Sz for the surfaces produced with the one-step strategy measure the larger number of peaks and valleys. The presence of the peaks on the surface may be due to the fluid dynamics in the melt track. Moreover, the height and depth of these were larger than in the case of surfaces produced with the one-step melting strategy. This is because the presence of the solid contour mitigates the material accumulation at the tail of the melt pool.

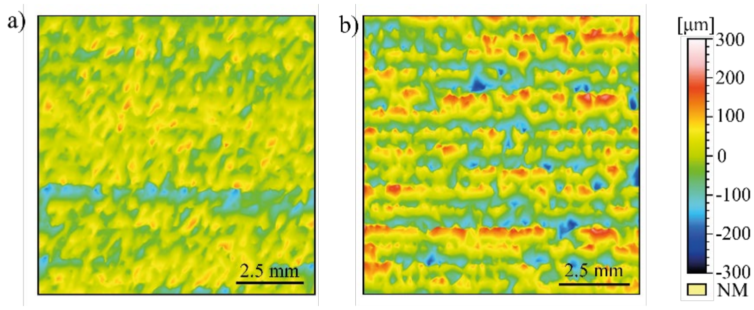


*Fig. 3: Topography analysis of the vertical surfaces: a) surface produced with two-step strategy, b) surface produced with one-step strategy.*

For the horizontal surfaces, the topography does not show a substantial difference between the two melt strategies, given similar values of average area roughness. For the surface produced using the two-step strategy Sa = 20 µm, while for the surface produced using the one-step strategy Sa = 22 µm.

Regarding the dimensional analysis, Fig. 4 shows the number of tolerance units obtained from the measures of the artefacts for the ISO base ranges considered in this work. The PBF-EB process for Ti4822 with the selected process parameters guarantees IT grades ranging from IT12 to IT16. The larger the feature of the sample, the higher the accuracy of the process (lower IT). For example, for the features comprising 1 mm and 3 mm, the PBF-EB process can guarantee an IT 16, while for larger features with dimensions from 80 mm to 120 mm, the PBF-EB process guarantees an IT 13. These values are comparable to other manufacturing processes, such as casting [18], which are usually compared to the PBF-EB technology. The melt strategies differ from each other only for a few ISO classes. Particularly, the samples produced with the one-step strategy has a higher dimensional accuracy (lower IT) then the samples produced with the two-step strategy for the classes 3mm – 6 mm and 6 mm – 10 mm (two-step process guarantees an IT 16 while, the one-step strategy can guarantee an IT 15), and in the base range 50 mm – 80 mm, for which the two-step strategy guarantees an IT 14, while the one-step strategy guarantees an IT 13.

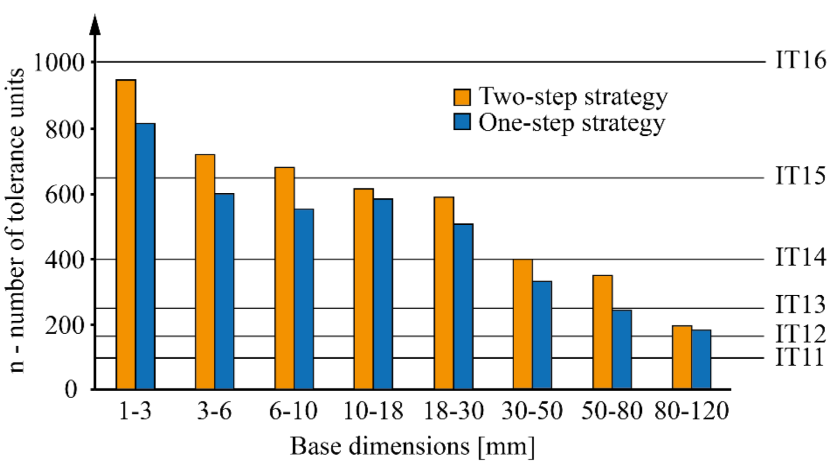


*Fig. 4. Number of tolerance units for the artefacts produced using the Two-step strategy and the one-step strategy for each ISO base dimensions.*

Fig. 5 shows the geometrical tolerance results for planarity and parallelism in an aggregate form as a box plot. Considering both planarity and parallelism, the melting strategy does not have a statistically relevant effect on the dimensional accuracy since all the boxes overlap. However, the two-step strategy has a beneficial effect on the planarity of the vertical surfaces, which shows a reduced median and interquartile range. The same applies to the parallelism of the vertical surfaces, where the vertical surfaces produced with a two-step strategy have a smaller median and an interquartile range below that of the vertical surface produced with the one-step strategy. These results agree with the results obtained from the topography analysis of vertical surfaces reported in Section 3.1. The difference in the dimensional accuracy among the melting strategies could be related to the larger peaks and valleys and larger values of surface roughness for vertical surfaces produced with the one-step strategy.

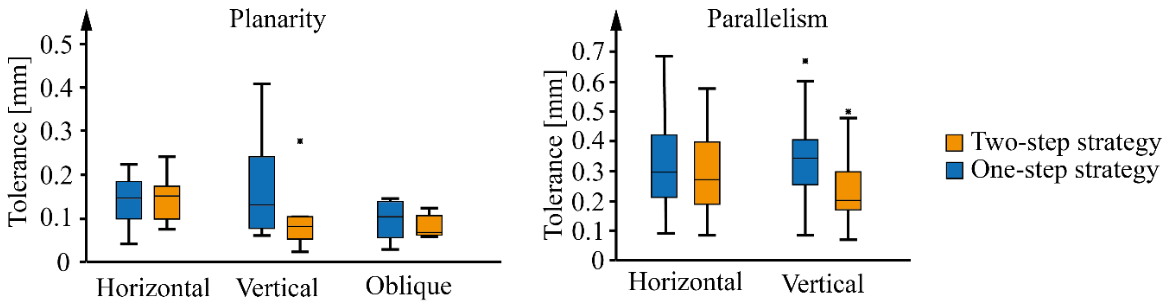


*Fig. 5. Geometrical tolerances for planarity and parallelism*

Fig. 6 a) summarises the tolerance data for the perpendicularity, coaxiality and cylindricity as box plots for the two melt strategies. The box plot shows that the melting strategy is not statistically relevant to the perpendicularity, coaxiality and cylindricity. Regarding the coaxiality, although the overlapping of the boxes, the median and the interquartile range obtained for the features produced using the two-step strategy are smaller than those produced using the two-step strategy. This means that, on average, the two-step strategy produced better coaxiality of the features. Fig. 6 b) shows the box plots for the tilt angles of the surfaces with respect to the coordinate axes defined in Fig. 1. In this case, for the deviation with respect to the X-axis and the deviation with respect to the Z-axis, the melting strategy is statistically relevant. The two-step strategy produces surfaces tilted with a smaller deviation with respect to the coordinate axes. On the other hand, the melting strategy does not have a statistically relevant effect on the deviation of the tilt angle with respect to the Y-axis. While the interquartile range is comparable for the two-step and the one-step strategy, the median of the two-step strategy is smaller, and the box shows smaller deviation values. However, the interquartile range for surfaces produced with the two-step strategy goes at negative values, while this never happens for surfaces produced with the one-step strategy.

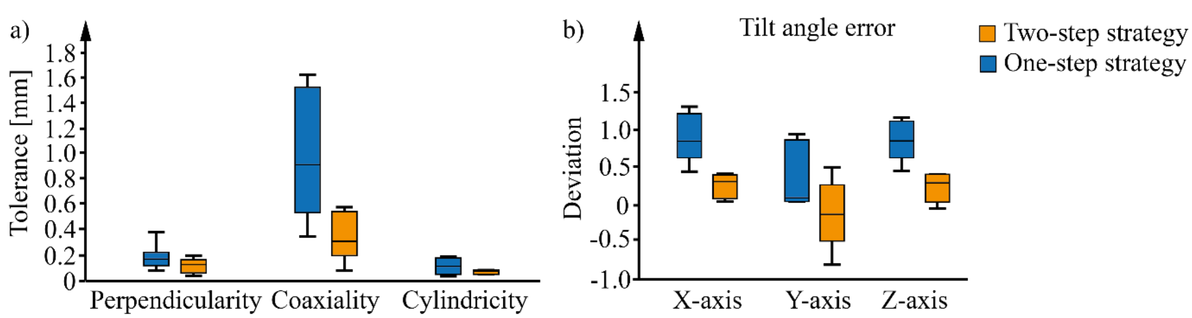


*Fig. 6. (a) Tolerance for Perpendicularity, coaxiality and cylindricity and (b) Deviation of the angles with respect to the coordinate axes.*

**Conclusions**

The PBF-EB process enables easier processing of γ-TiAl Ti48Al2Cr2Nb compared to other methods, making it suitable for aerospace, biomedical, and automotive applications. This study examines the impact of one-step and two-step melting strategies on surface topography and dimensional accuracy. The two-step strategy improves surface smoothness and reduces staircasing effects but requires 8% more processing time. Dimensional accuracy analysis shows that PBF-EB achieves IT12–IT16 grades, with larger features exhibiting higher precision. The one-step strategy ensures a faster production of parts, making it preferable for aerospace and automotive applications that usually require post-processing operations. The two-step strategy, with proper correction, may be suited for biomedical components where as-built roughness is acceptable. Selecting the appropriate melting strategy is crucial for balancing surface quality, dimensional accuracy, and post-processing needs. These results provide guidelines for determining whether PBF-EB alone meets tolerance requirements or if machining is necessary, aiding process optimisation and simulation-based geometric compensation.

## References

[1] W. Chen and Z. Li, 11 - Additive manufacturing of titanium aluminides, in Additive Manufacturing for the Aerospace Industry, F. Froes and R. Boyer, Eds., Elsevier, 2019, 235–263. https://doi.org/10.1016/B978-0-12-814062-8.00013-3

[2] R. Wartbichler, H. Clemens, S. Mayer, C. Ghibaudo, G. Rizza, M. Galati, L. Iuliano, et al., On the Formation Mechanism of Banded Microstructures in Electron Beam Melted Ti–48Al–2Cr–2Nb and the Design of Heat Treatments as Remedial Action, Advanced Engineering Materials, 23, (2021), 2101199, https://doi.org/10.1002/adem.202101199

[3] M. Galati, Chapter 8 - Electron beam melting process: a general overview, in Additive Manufacturing, J. Pou, A. Riveiro, and J. P. Davim, Eds., in: Handbooks in Advanced Manufacturing, Elsevier, 2021, 277–301. https://doi.org/10.1016/B978-0-12-818411-0.00014-8

[4] G. Rizza and M. Galati, Powder bed fusion with electron beam: The interplay of sintering, porosity, and coordination number in modelling the powder thermal conductivity through a novel tortuosity formulation, International Journal of Heat and Mass Transfer, 234, (2024), 126055, https://doi.org/10.1016/j.ijheatmasstransfer.2024.126055

[5] P. Wang, W. J. Sin, M. L. S. Nai, and J. Wei, Effects of Processing Parameters on Surface Roughness of Additive Manufactured Ti-6Al-4V via Electron Beam Melting, Materials, 10, (2017), Art. no. 10, https://doi.org/10.3390/ma10101121

[6] M. Galati, G. Rizza, S. Defanti, and L. Denti, Surface roughness prediction model for Electron Beam Melting (EBM) processing Ti6Al4V, Precision Engineering, 69, (2021), 19–28, https://doi.org/10.1016/j.precisioneng.2021.01.002

[7] M. Galati, S. Defanti, A. Saboori, G. Rizza, E. Tognoli, N. Vincenzi, A. Gatto, et al., An investigation on the processing conditions of Ti-6Al-2Sn-4Zr-2Mo by electron beam powder bed fusion: Microstructure, defect distribution, mechanical properties and dimensional accuracy, Additive Manufacturing, 50, (2022), 102564, https://doi.org/10.1016/j.addma.2021.102564

[8] C. Körner, Additive manufacturing of metallic components by selective electron beam melting — a review, International Materials Reviews, 61, (2016), 361–377, https://doi.org/10.1080/09506608.2016.1176289

[9] C. Pirozzi, S. Franchitti, R. Borrelli, G. Diodati, and G. Vattasso, Experimental Study on the Porosity of Electron Beam Melting-Manufactured Ti6Al4V, J. of Materi Eng and Perform, 28, (2019), 2649–2660, https://doi.org/10.1007/s11665-019-04038-7

[10] P. Karimi, C. Schnur, E. Sadeghi, and J. Andersson, Contour design to improve topographical and microstructural characteristics of Alloy 718 manufactured by electron beam-powder bed fusion technique, Additive Manufacturing, 32, (2020), 101014, https://doi.org/10.1016/j.addma.2019.101014

[11] A. L. Cooke and J. A. Soons, Variability in the Geometric Accuracy of Additively Manufactured Test Parts, (2010), Accessed: Oct. 27, 2024. Available: https://hdl.handle.net/2152/88219

[12] P. Minetola, L. Iuliano, and G. Marchiandi, Benchmarking of FDM Machines through Part Quality Using IT Grades, Procedia CIRP, 41, (2016), 1027–1032, https://doi.org/10.1016/j.procir.2015.12.075

[13] ISO 286:1988 ISO system of limits and fits. Part 1 Bases of tolerances deviations and fits, 286–1:1988, (1988).

[14] BS EN ISO 286-1:2010 Geometrical product specifications (GPS). ISO code system for tolerances on linear sizes. Basis of tolerances, deviations and fits, 286–1:2010, (2010). Available: https://bsol.bsigroup.com/Bibliographic/BibliographicInfoData/000000000030288630

[15] Benchmarking of Additive Technologies | 3D CAD Model Library | GrabCAD. Accessed: Feb. 02, 2025. Available: https://grabcad.com/library/benchmarking-of-additive-technologies-1

[16] J. Bieske, M. Franke, M. Schloffer, and C. Körner, Microstructure and properties of TiAl processed via an electron beam powder bed fusion capsule technology, Intermetallics, 126, (2020), 106929, https://doi.org/10.1016/j.intermet.2020.106929

[17] S. Biamino, A. Penna, U. Ackelid, S. Sabbadini, O. Tassa, P. Fino, M. Pavese, et al., Electron beam melting of Ti-48Al-2Cr-2Nb alloy: Microstructure and mechanical properties investigation, Intermetallics, 19, (2011), 776–781, https://doi.org/10.1016/j.intermet.2010.11.017

[18] M. Grazia Violante, L. Iuliano, and P. Minetola, Design and production of fixtures for free-form components using selective laser sintering, Rapid Prototyping Journal, 13, (2007), 30–37, https://doi.org/10.1108/13552540710719190